Electrical Power and Energy Systems 119 (2020) 105892

Contents lists available at ScienceDirect

Electrical Power and Energy Systems

journal homepage: www.elsevier.com/locate/ijepes

Extended operating range of PV module-level CHB inverter

Marino Coppola*, Pierluigi Guerriero, Diego Iannuzzi, Santolo Daliento, Andrea Del Pizzo

Department of Electrical Engineering and Information Technologies, University of Napoli – Federico II, Italy

ARTICLE INFO

Keywords:
Photovoltaic power system
CHB inverter
Hybrid Modulation
Distributed MPPT

ABSTRACT

In this paper an enhanced distributed maximum power point tracking (DMPPT) algorithm, along with an improved hybrid modulation method for a photovoltaic (PV) module-level Cascaded HBridge (CHB) inverter, is proposed. The advantages and drawbacks of the CHB topology in distributed PV generation systems are highlighted. The main benefits are related to the higher granularity of the PV power control, which mitigates mismatch effects, thus increasing the power harvesting. Nevertheless, heavy unbalanced configurations need to be properly addressed by means of dedicated control action. The proposed control strategy allows to overcome the operating limits of PV CHB inverter, by integrating in the MPPT algorithm a limitation of the individual cell modulation index. Experimental tests carried out on a laboratory prototype of a singlephase sevenlevel PV CHB inverter, evidence the effectiveness of the proposed control and modulation approach in terms of extended operating range and MPPT efficiency.

1. Introduction

Nowadays, the green power generation is an ever-growing challenge. In fact, the demand of electricity production from renewable sources is growing continually to reduce the environmental pollution, global warming and, contextually, the use of fossil fuels. Among the different renewable sources, solar energy has assumed a relevant role in order to match the electricity demand so leading to additional issues to be solved for its optimal integration into the grid [1]. This latter can be reached by means of power converters which represent the interface between renewable-energy sources and electrical grid [2], with the aim of ensuring not only a maximum sun energy harvesting, through a Maximum Power Point Tracking (MPPT), but also high output power quality to meet the grid code [3].

In particular, gridtied photovoltaic (PV) systems [4], depending on PV module arrangement, can be classified in (i) string, (ii) multistring, (iii) arrays and (iv) single module. Different module arrangements lead to correspondingly different inverter configurations: (i) string, (ii) multistring, (iii) central and (iv) ac-module inverter [5].

Centralized, string and multistring PV system architectures (i.e., structures based on PV sources consisting in modules connected in series) suffer from reduced power generation in case of mismatch due to partial shading, and uneven ageing of PV modules. In fact, in these circuit topologies, lower performance of an individual PV module can affect the performance of the whole system. This latter issue can be overcome by exploiting ac-module topologies, which were introduced for single module application with the aim of avoiding mismatch losses. Improved results achievable by ac-module topologies are due to the chance of build up distributed power generation systems (DPGS), allowing distributed MPPT (DMPPT), which means improved MPPT capabilities and modularity [6–10]. Aforementioned architectures usually consist of two power stages: a dc-dc converter, to obtain proper voltage boost and/or wider MPP tracking, followed by a dc-ac inverter to interface the PV sources with the grid. The drawback of this inverter arrangement is that the conversion efficiency is adversely affected by the doublestage configuration and by the high voltage stepup ratios needed for the grid connection. A feasible way to realize a distributed PV module converter architecture avoiding the multi-stage boost configuration is represented by the multilevel topology, which typically exploits single dc/ac power conversion stage for each PV source, also in the case of transformerless grid-tie application [11]. Moreover, a multilevel conversion circuit, thanks to its inherent nature, also accomplishes with the concept of DER (Distributed Energy Resources) which is strictly related to the development of future mixed grid [12].

Among multilevel circuit topologies, the cascaded H-Bridge (CHB) has assumed a relevant role in PV applications [13–25]. Its wellknown general features are [26,27]: the separate dc-link for each power cell; the modular structure (allowing the sharing of voltage boosting among the power cells forming the cascade); the multilevel output voltage waveform with a number of voltage steps depending on the number of cells; the higher equivalent switching frequency, which increases with the number N of cells. This latter characteristic ensures better quality of

* Corresponding author at: Via Claudio, 21, 80125 Napoli, Italy.
E-mail address: marino.coppola@unina.it (M. Coppola).

https://doi.org/10.1016/j.ijepes.2020.105892
Received 18 March 2019; Received in revised form 10 October 2019; Accepted 27 January 2020
Available online 05 February 2020

the output (e.g., reduced total harmonic distortion (THD)) and weaker requirements for the line filter.

In principle, the peculiarities of the CHB architecture allow to implement a distributed modulelevel inverter with DMPPT capabilities, which guarantees the maximization of the energy harvested from each PV generator (i.e., PV module) [19], even under mismatch conditions among PVGs. For this purpose, the control system must be able to handle unbalanced power of the cells to meet different operating conditions of the PV generators. The possibility of allowing uneven operation of PV generators is one of the main issues to be addressed for this circuit topology. In fact, in a cascade structure the H–Bridge cells are connected in series, so sharing the same output current, while the power delivered by each cell is directly related to the amplitude of its voltage modulation index. In other words, the cells which must handle a larger PV power, with respect to the others, operate with higher modulation indexes [15–17,20,21]. Under deep mismatch, the modulation index of the most powerful cell could increase up to exceed the unity, so reaching the overmodulation region. Conventional modulation strategies (e.g., Multicarrier PWM) cannot achieve modulation index higher than unity due to the degradation of the output current THD, as clearly stated in [20,21].

Nevertheless, overmodulation can be exploited to extend the operating range of the inverter in case of deep mismatch. In such a case, the modulation index could be theoretically increased up to $4/\pi$ (i.e., square-wave modulation), which represents the maximum power capacity of a cell. A further power raise cannot be handled by the cell itself, thus any power excess is only transferred to the dclink capacitor, whose voltage increases, so determining a difference between the MPP voltage reference and the actual dclink voltage [20]. Obviously, this means that the cell cannot longer track the MPP reference, thus leading to a lack of the control action. The possibility of achieving the maximum power capacity of a cell depends on the used control strategy, where the modulation technique must be properly conceived to allow CHB inverter operation also in overmodulation region.

In the recent literature, many conventional methods have been modified to handle unbalanced dc sources: multicarrier PWM approach [13–16,18,19,21], reactive power control [17], nonactive power control [22], selective harmonic elimination (SHE) [23]. However, these methods cannot manage heavy power imbalance without affecting system control and power quality (i.e., strongly distorted output waveforms). In particular, as conventional methods, modified approaches using multicarrier PWM (except [23]) cannot exploit an extended modulation index range. So, under deep mismatch conditions, the strict constraint on the unity upper boundary of modulation indexes does not allow correct MPPT, thus exacerbating the tradeoff between MPPT efficiency, controllability and THD.

In [20] a hybrid modulation method based on [25], along with a derivativeofpower based control method, is used to take advantage of CHB cells full potential and to stabilize the CHB inverter under heavy mismatch conditions, but the implementation of the proposed technique can result difficult because of using the derivative of PV power [21].

In this paper, the hybrid modulation method proposed by the authors in [25] is used in its improved version presented in [28], along with an enhanced MPPT algorithm, which includes the modulation index control of [16] properly modified to allow a cell to work in the overmodulation region (by fixing an upper limit for the modulation index greater than one), so overcoming the constraint on the unity modulation index of the conventional control strategies. This latter is only possible thanks to the proposed hybrid modulation method, which allows only one cell to work in switching mode (i.e., PWM mode), while the others are kept in fixed states: 0 mode, corresponding to a cell bypassed (i.e., its output voltage is zero); ± 1 mode, corresponding to a cell inserted (i.e., its output voltage is equal to the dc-link voltage). So, unlike the modulation scheme of [20], the proposed technique performs a dedicated mixed staircase-PWM strategy which carries out four possible states for a cell: 0, ± 1, PWM, but only one cell is in PWM, while the other cells provide a constant output voltage. In such a way, it is possible to extend the operating range of a distributed PV modulelevel CHB architecture or rather the system can fully operate also in heavy mismatch conditions, with no detrimental effect on the harmonic content of the output current (i.e., grid current) and ensuring optimal performance in terms of MPPT efficiency.

In the following sections, numerical analysis and experimental tests, carried out on a singlephase sevenlevel PV CHB inverter, are presented to validate the effectiveness of the developed modulation and DMPPT techniques.

The paper is organized as follows. System description and principle of operation are presented in Section 2. The hybrid modulation method and the proposed control approach are reported in Section 3. A numerical analysis of system operation under different mismatch conditions is provided in Sections 4. Section 5 reports the experimental results to demonstrate the suitability of the proposed design and control approach. Conclusions are drawn in Section 6.

2. System description

The architecture of distributed PV modulelevel CHB inverter is shown in Fig. 1. It consists of N series connected power cells (i.e., H-Bridge circuits) forming a single stage dc/ac converter. A filter inductor L connects the dc/ac converter output to the grid, in order to allow the injection of a sinusoidal current with unity power factor (PF). At the input of each cell, the power decoupling is achieved by means of the dclink capacitor C_i, properly sized to guarantee a reduced voltage ripple at the rated power level. A single PV module supplies each cell to realize a DPGS.

The main quantities describing the operation of the circuit can be defined as follows. The inverter ac output voltage is

$$v_{inv} = \sum_{i=1}^{N} v_{Hi} \tag{1}$$

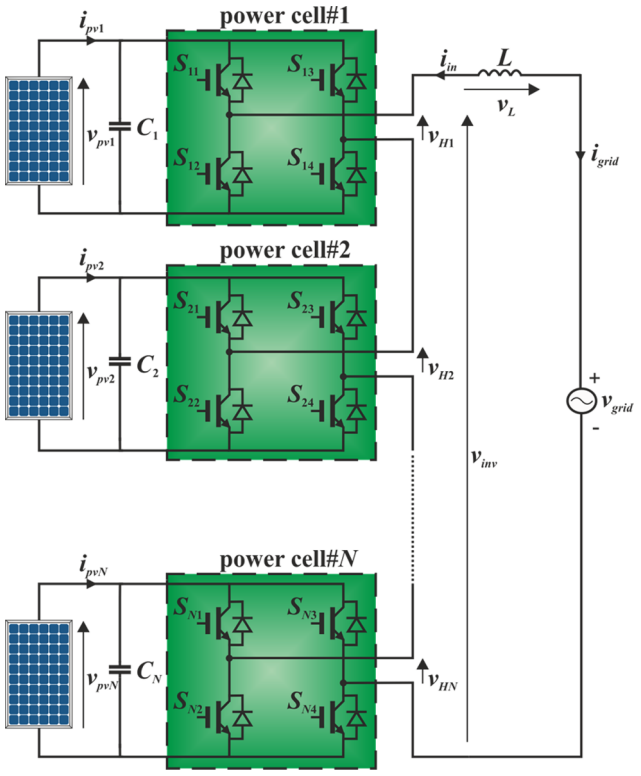

Fig. 1. Architecture of $2N$ + 1-level grid-tied PV module-level CHB inverter.

where v_{Hi} represents the output of i-th cell and can be easily expressed as

$$v_{Hi} = (S_{i1} - S_{i3})v_{pvi} = h_i v_{pvi} \quad i = 1, ...,N \tag{2}$$

$S_{i,j}$ being the logic state of the j-th switch in the i-th cell; the switch conducts when $S_{i,j} = 1$, while is off when $S_{i,j} = 0$. By considering $S_{i,1} = \bar{S}_{i,2}$ and $S_{i,3} = \bar{S}_{i,4}$, under unipolar PWM, the control signal h_i can assume three discrete values: $+1$ (i.e., $S_{i,1} = 1$ and $S_{i,3} = 0$), -1 (i.e., $S_{i,1} = 0$ and $S_{i,3} = 1$), 0 (i.e., $S_{i,1} = S_{i,3}$).

By replacing h_i with a continuous switching function s_i (i.e., modulating waveform), the system dynamics can be modeled as follows:

$$\begin{aligned} &\frac{di_{in}}{dt} = \frac{v_L}{L} = \frac{v_{grid} - v_{inv}}{L} = \frac{v_{grid} - \sum_{i=1}^{N} s_i v_{pvi}}{L} \\ &\frac{dv_{pvi}}{dt} = \frac{1}{C_i}(i_{pvi} + s_i i_{in}) \qquad i = 1, ...,N \\ &i_{grid} = -i_{in} \end{aligned} \tag{3}$$

The magnitude of the modulating waveform represents the modulation index:

$$m_i = \frac{v_{Hi,1}}{\bar{v}_{pvi}} \quad i = 1, ...,N \tag{4}$$

where $v_{Hi,1}$ is the fundamental component of v_{Hi} and $\bar{v}_{pvi}$ is the mean value of v_{pvi}. In Section 4, the dependency of m_i on the operation of the other cells is discussed in order to evidence the operating limits of the whole converter in case of mismatch.

3. Control implementation

The control scheme, for the application under study, is shown in Fig. 2. It consists of four stages [7]: the MPPT stage, the dc voltage control, the power/current control and the modulator stage. As can be seen, the first stage performs dedicated MPPT controllers, which provide individual MPP voltage reference of each PV module, based on P&O algorithm, and dynamic control of operating voltage and modulation index. The second and the third stages perform the main control by generating the inductor current reference i_{in}^{ref} and the inductor voltage reference v_L^{ref}. The modulator stage supplies the driving signals for the power cells by means of an improved hybrid modulation technique; it embeds a sorting algorithm selecting which cell is to be driven in PWM mode. The detailed description of each stage is reported in the following subsections.

3.1. Main inverter control strategy

The main inverter control, performed by the second and third stages, is designed to ensure the transfer of the active power from PV modules to the grid with unity power factor and low distortion. As shown in Fig. 2, the main control loop is unique because of the series connection of the H-bridge cells, which means that the output current is the same for each of them. The control action is performed by using a dualloop controller (i.e., cascade of two PI controllers) [29]. The outer loop regulates the sum of dclink voltages to obtain the amplitude of the current reference. This latter is then multiplied by the PLL output in order to provide a sinusoidal current reference in phase with grid voltage (i.e., unity power factor). The inner loop provides the reference inductor voltage, v_L^{ref}, which subtracted from the grid voltage, gives the inverter voltage reference, v_{inv}^{ref}. This latter quantity is the input of the modulator stage, where hybrid modulation achieves individual dclink control or rather contributes to the individual MPP tracking. In fact, it is obtained by means of two different mechanisms, namely, (1) the outer overall dc-link voltage control loop and (2) the voltage error control due to the sorting algorithm. The former acts by regulating the output current amplitude in order to reduce the average overall dc-link voltage error, while the latter provides the operating modes of each cell in order to individually track the MPP voltage references. As an example, even if the overall dc-link voltage error (i.e., $\sum_{i=1}^{N} v_{pvi}^{ref} - \sum_{i=1}^{N} v_{pvi\_f}$, see also Fig. 2) is close to zero, due to the compensation of positive and negative errors, which means that this control loop does not act to further regulate the output current, nevertheless the sorting algorithm, performed in the modulator stage, allows to individually track the MPP voltage reference of each cell, as detailed in Section 3.3.

Then, it must be considered that the execution time of the sorting algorithm is much smaller than MPPT period, thus ensuring that, in each MPPT period, the cells can change their switching state hundred times in order to track the desired MPP voltage reference.

Finally, it is worth highlighting that the use of a PR in the inner control loop (i.e., the current controller) is high advisable because of its ability of zeroing the steady-state error at the fundamental frequency. Moreover, a reactive power control should be implemented to satisfy the grid code requirements, as in [28], where the authors applied the proposed approach to a threephase PV CHB inverter. Nevertheless, in this work, the authors chose to simplify the control scheme and to restrict the operation of the inverter to power injection with unity power factor, in order to focus the attention on the extended operating range under mismatch conditions.

Nevertheless, in this particular application, the main objective is to verify the extended operating range of the PV CHB inverter, and a PI controller does not affect the desired results, while ensuring adequate performance in terms of output power quality.

3.2. Distributed MPPT

The proposed DMPPT approach consists in a dedicated MPPT control stage for each power cell. As described in Fig. 3, each stage performs a fixed-step perturbation of the reference voltage v_{pvi}^{ref}. The perturbation sign is chosen by a multiplexer, whose selection signal is derived from the logic OR among the output of a P&O algorithm, and the output of two specific control checks (comp #1 and #2). The corresponding output is set to 1 when the MPP voltage is supposed to be larger than the reference voltage, and to 0 otherwise. The iteration period is equal to 50 ms and the voltage reference step is $\Delta_{pv} = 0.5$ V.

The P&O block receives as inputs the measured PV voltage and current, properly filtered by means of a 100 Hz bandstop digital filter. This latter cuts off the 100 Hz ac oscillation inherently due to dc/ac conversion. The main purpose of placing the 100 Hz filter between the measured dclink voltages (i.e., v_{pvi} $i = 1,..,N$) and the main controller

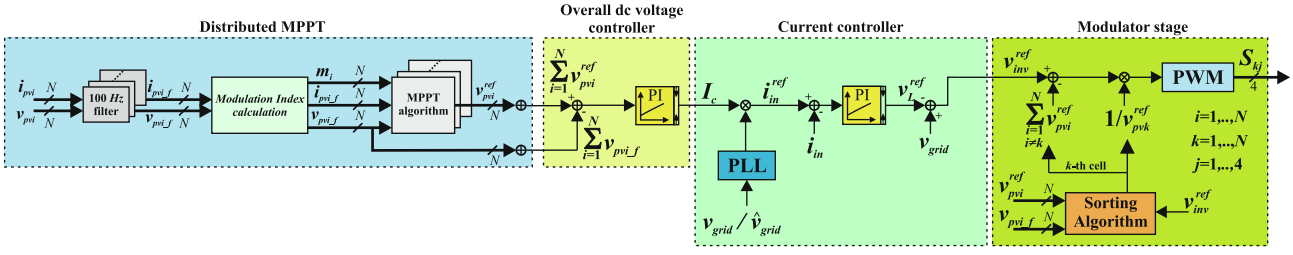

Fig. 2. Proposed control scheme.

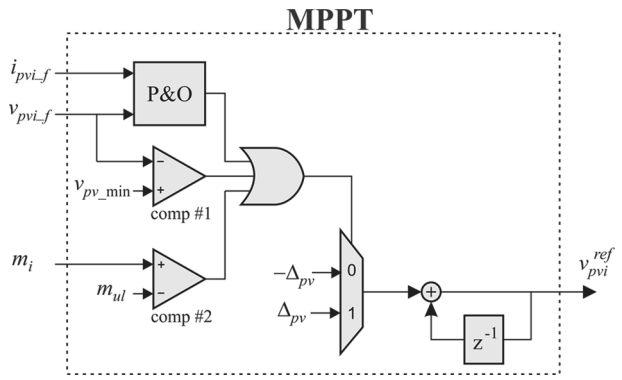

Fig. 3. Logic circuit describing the MPPT for the i-*th* cell.

inputs (see Fig. 2) is avoiding the presence of third harmonic in the output current reference [13]. Nevertheless, the injection of third harmonic voltage and current is unavoidable and the PI does not allow to avoid this issue, also if, as aforementioned, this does not invalidate the obtained results.

Moreover, in order to guarantee that the overall dc voltage (i.e., the sum of the cells' dc-link voltages) be always greater than the grid peak voltage, a lower boundary, v_{pv_min}, for the MPP tracking range of individual cells, at least greater than the grid peak voltage divided by N, was assumed. If the voltage reference v_{pvi}^{ref} is lower than the v_{pv_min}, the output of comparator #1 (see Fig. 3) goes high, thus leading to a positive increment of the voltage reference, regardless to the P&O output. It should be noted that the definition of the MPP tracking range poses control issues; for example, the operation of a solar panel in the flat region of the IV curve (i.e., where the PV panel behaves as constant current generator) should be prevented. This further constraint was taken into account in the choice of v_{pv_min}, based on the IV characteristic of the used PVG.

In addition to that, a control of the modulation index is exploited starting from the method proposed in [16]. By considering Eqs. (1)–(4), the relationship between the modulation index and the main circuit parameters can be derived. By taking in mind Eq. (3), we can write:

$$i_{pvi} - C_i \frac{dv_{pvi}}{dt} = s_i i_{grid} \tag{5}$$

and by considering the average quantities at steadystate, it can be easily obtained

$$\bar{i}_{pvi} = \frac{1}{2} m_i I_{grid} \cos\varphi \tag{6}$$

where I_{grid} is the amplitude of grid current, while $\cos\varphi$ is the power factor. Moreover, the average power balance, in an ideal lossless system and neglecting higher harmonic content, can be expressed as:

$$P_{in,ave} = \sum_{i=1}^{N} \bar{v}_{pvi} \bar{i}_{pvi} = \frac{1}{2} V_{grid} I_{grid} = P_{out,ave} \tag{7}$$

where V_{grid} is the amplitude of the grid voltage and $P_{out,ave}$, $P_{in,ave}$ are the average total output power and the dc total input power, respectively. As a consequence, in case of steadystate at unity power factor ($\cos\varphi = 1$) Eq. (6) can be rewritten as:

$$m_i = \frac{2\bar{i}_{pvi}}{I_{grid}} \tag{8}$$

By substituting the value of I_{grid} extracted from Eq. (7), it can be established the following relationship:

$$m_i = \frac{V_{grid}}{\sum_{j=1}^{N} \bar{v}_{pvj} \frac{\bar{i}_{pvj}}{\bar{i}_{pvi}}} \quad i = 1, \ldots, N \tag{9}$$

From Eq. (9), it can be inferred that the modulation indexes mainly depend on the ratio i_{pvj} / i_{pvi}, thus if the irradiance of ith power cell decreases, w.r.t. the other cells, its modulation index decreases, while it increases as the cell is subjected to an increasing irradiance.

Eq. (9) is implemented in the control, thus providing the instantaneous value of m_i as input to the MPPT block. If m_i overcomes the allowed upper limit m_{ul} the output of comparator #2 (see Fig. 3) goes high, thus leading to a positive increment of the voltage reference, regardless to the P&O output. As a consequence, the corresponding modulation index m_i decreases.

In order to avoid lack of system control and high distorted current, the algorithm proposed in [16] fixes the upper limit of the modulation index to 1, corresponding to the circuit operation in the linear modulation zone. So, if the modulation index of a cell overcomes the unity boundary, the algorithm stops performing the P&O and increases the cell voltage v_{pvi} (i.e., reduces the current i_{pvi}) until the modulation index becomes lower than unity.

In our case, the proposed hybrid modulation method allows modulation indexes greater than one, since, as described in the next section, only one cell per cycle is in PWM mode unlike conventional modulation techniques [20]. As a consequence, the operating region can be enlarged, thereby allowing each cell to handle its own PV power also in case of deep mismatch among the PV modules. This means that the PV CHB inverter becomes able to properly operate in a higher number of mismatch configurations of cells, so improving the system performance. The upper limit m_{ul} is greater than 1 and its maximum achievable value depends on the adopted modulation strategy. The identification of such limit will be discussed in Section 5.

3.3. Hybrid Modulation Method

The proposed hybrid modulation method is based on an adaptive algorithm which divides, at every control step (i.e., the execution time period of the proposed algorithm), the inverter output voltage reference v_{inv}^{ref} in N intervals (N being the number of cells in the cascade). Due to

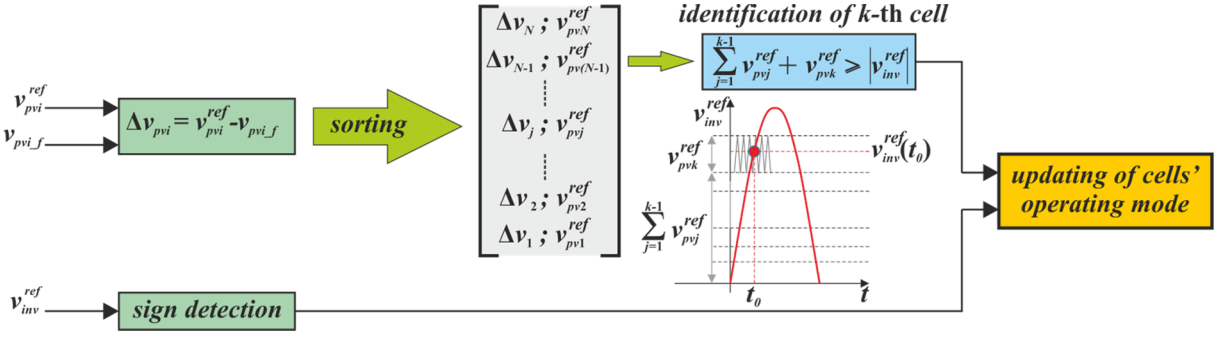

Fig. 4. Scheme of sorting algorithm.

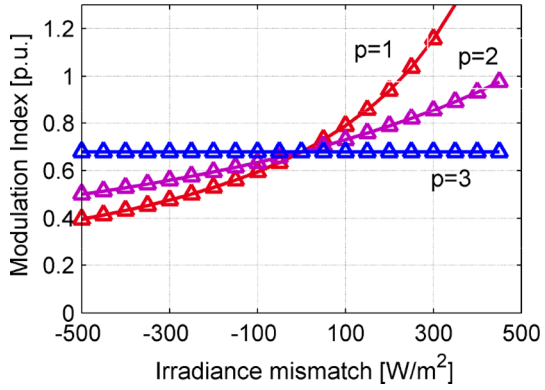

Fig. 5. Modulation indexes ($N = 3$): behavior of modulation index w.r.t. the irradiance mismatch for different mismatch configurations (p = 1, 2, 3).

the different values of the MPPT voltage references (v_{pvi}^{ref}), each interval has different amplitude. More in details (see Fig. 4), the input data for the adaptive algorithm are: the MPPT voltage references, v_{pvi}^{ref}; the filtered measured dclink voltages, v_{pvi_f}; the inverter voltage reference, v_{inv}^{ref}. The first step is the calculation of the voltage error at each dclink as the difference between MPPT voltage reference and the filtered measured dclink voltage. A positive error means that the cell dclink must be charged. Consequently, the cell is bypassed (i.e., 0 mode), so allowing the PV source to charge the corresponding dclink, meanwhile, the cell output voltage v_{Hi} is zero. Conversely, a negative error means that cell dclink must be discharged to track the desired reference. To this end, the cell is inserted (i.e., ± 1 mode), so the corresponding dclink can be discharged; meanwhile the cell output voltage is equal to $\pm v_{pvi}$ (the sign depends on the detected sign of v_{inv}^{ref}). After the voltage errors calculation, a sorting procedure is applied to obtain an ordered vector, where the first element (i.e. #1) is associated to the cell with the lowest negative error, while the last element (#*N*) is associated to the cell with the highest positive error. It worth noting that the ordering index *j* does not correspond to the physical position of the cells in the cascade (as per the index *i*). Each element of the sorted vector consists of pair made by the cell voltage error and the corresponding MPPT voltage reference (i.e., the desired voltage at the dclink). After that, the cell, to be driven in PWM mode, is identified by means of an iterative procedure. This latter performs the sum of the MPPT voltage references, starting from the first position of the sorted vector, until the index *k*, verifying the following relationship is found.

$$\sum_{j=1}^{k-1} v_{pvj}^{ref} + v_{pvk}^{ref} \geq |v_{inv}^{ref}| \tag{10}$$

To properly synthesize the inverter multilevel waveform, the first *k*-1 cells of the sorted vector will be kept in discharging mode (± 1 mode), the *k*th cell will be driven in PWM mode, whereas the remaining *N*-*k* cells will be bypassed (0 mode corresponding to the charging mode). The updated control signals do not change until the next execution of the sorting algorithm, whose time step T_{sort} is chosen greater than the switching period T_{sw}. It is worth noting that the sorting algorithm, at steady state, allows to discharge the most powerful cells by assigning them an index $j \leq k$. When a single cell exhibits a producible power significantly larger than the others, that cell is nearly always kept in +1 mode in the positive half-cycle and −1 mode in the negative half-cycle, thus tending to the square wave operation. Nevertheless, the cell cannot achieve a full square wave operation because it must be operated in PWM mode at least when $k = 1$. On the contrary, the control proposed in [20] allows to reach a full square wave operation because it never uses the 0 mode, while always keeping at least one cell in +1 mode in the positive half-cycle and −1 mode in the negative half-cycle.

4. Extended operating range analysis

This section is devoted to identify the boundaries of the extended operating region of a distributed PV modulelevel CHB inverter. This architecture allows independent voltage control and ensures individual MPPT at each dclink. Indeed, in normal operating condition each cell of the cascade can handle its corresponding power, while ensuring stably tracking of the MPP. However, in case of heavy mismatch, the cells with the higher power content could be not able to work at the MPP. In fact, the cells with the lower power limit the injected current, thus forcing the cells with higher power to drift away from the MPP towards higher voltages (i.e., higher power cells towards a higher voltage, lower power cells towards a lower voltage) until reaching a new condition, where the corresponding power can be tolerated by the cell. Therefore, a reduction of overall power production is the price to pay to guarantee extended inverter operating range.

The following analysis gives a deeper insight into the effect of mismatch on inverter operation. For the sake of generality, the analysis does not refer to a particular modulation strategy. The obtained results are carried out by properly implementing a Matlab code to solve Eq. (9) taking into account the constraints imposed by the P-V curve and the PV voltage operating range [v_{pvmin} = 24.5 V ÷ V_{oc} = 35 V]. In fact, Eq. (9) represents the necessary and sufficient analytical expression to address the interaction among the cells in mismatch conditions.

Let's consider a CHB inverter made of *N* cells, each powered by a PV module. Initially, all modules were subject to an irradiance of 500 W/m^2. Then, in order to investigate the effect of mismatch, the irradiance of *p* modules was kept constant, while the irradiance of the other *N*-*p* modules was linearly varied in the range [50 W/m^2 ÷ 1000 W/m^2].

The behavior, for $N = 3$ (i.e., seven-level CHB), of the modulation indexes m_i, corresponding to the *p* cells, is reported in Fig. 5, where the irradiance mismatch is defined as the difference between the constant irradiance of the *p* modules and the varying irradiance of the remaining *N*-*p*. Thus, the x-axis span over the range −500 W/m^2, +450 W/m^2 (i.e., (5001000) *W/m*^{2}, (50050) *W/m*^{2}). Under uniform condition (i.e., $p = 3$), the modulation index is constant and, as expected, the same for all the three cells. In case of mismatch ($p < N$), the modulation index is a monotonic increasing function of the irradiance mismatch. In particular, positive mismatches drive the more powerful cells in overmodulation, thus affecting the performance of the whole system. The slope of m_i increases as the number *N*-*p* of uneven irradiated modules increases, thus suggesting that the inverter can properly operate under a reduced number of irradiance mismatch configurations. The effect of mismatch in the worst case ($p = 1$) is exacerbated when the number *N* of cells increases, as shown in Fig. 6 for the cases $N = 1 \div 10$.

In order to ensure an extended operation of the system, a specific control strategy must be implemented. The approach proposed in [16] fixes the modulation index limit to unity. Unfortunately, the cells

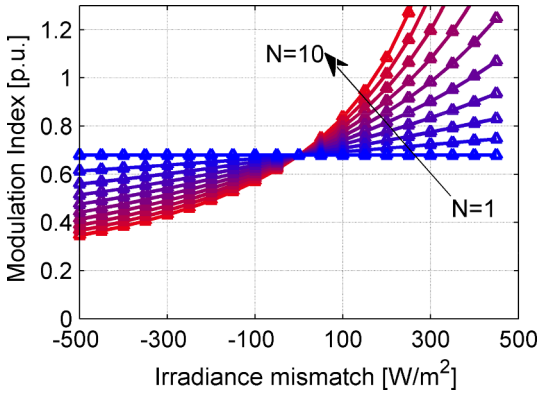

Fig. 6. Modulation indexes (w.c., p = 1): behavior of modulation index w.r.t. the irradiance mismatch for different number of cells.

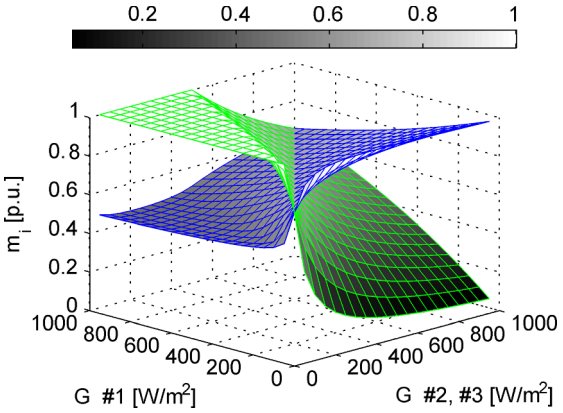

Fig. 7. Modulation indexes ($N = 3$): irradiance level of module #1 independently varies with respect to module #2 and #3.

subject to this limitation are not able to properly track the MPP of the corresponding PV module, thus affecting the global MPPT efficiency.

In order to point out the MPPT efficiency degradation, let's refer to the $N = 3$ topology. By following a combinatorial approach, the irradiation level of module #1 was varied independently with respect to module #2 and #3 (i.e., module #2 and #3 were always subject to the same irradiance).

In Fig. 7 the behavior of modulation indexes of the three power cells is reported (m_1 being the green surface; m_2 and m_3 being the same blue surface), while the corresponding global MPPT efficiency is shown in Fig. 8. In the region where the irradiance of module #1 prevails with respect to module #2 and #3, the control acts to keep $m_1 < 1$. Unfortunately, this action affects the MPPT efficiency, which significantly degrades in that region. According to that analysis, it is not possible to perform individual MPPT for the PV sources of a CHB in case of deep mismatch.

Fig. 9 shows the effect of mismatch on the MPPT efficiency when the module #1 is subject to a constant irradiation level of 1000 W/m^2, while module #2 and #3 experience the same irradiation varying in the range [200 W/m^2, 1000 W/m^2]. The irradiance mismatch is defined as the difference between the constant irradiance of the module #1 and the varying irradiance of the remaining modules #2 and # 3. Thus, the x-axis span over the range 0 W/m^2, +800 W/m^2 (i.e., (10001000) *W/m^2*, (1000200) *W/m^2*). As the mismatch increases, the modulation index of cell #1 increases, reaching the unity value at about 500 W/m^2 (i.e., irradiance mismatch of 500 W/m^2). In this condition, cell #1 still operates at MPP. Conversely, in case of larger mismatches, the control forces the operating voltage of module #1 to increase w.r.t. the MPP voltage, thus avoiding the modulation index to exceed the unity

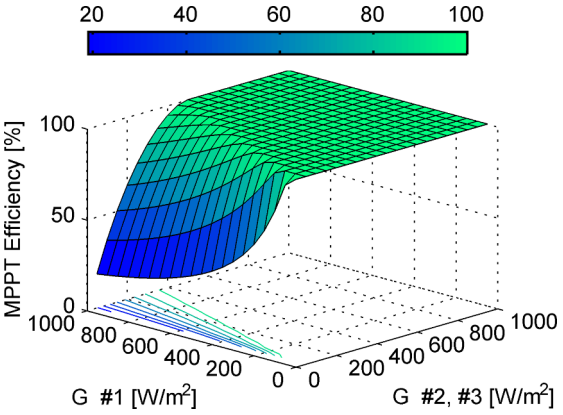

Fig. 8. MPPT efficiency ($N = 3$): irradiance of module #1 independently varies with respect to the irradiance of module #2 and #3.

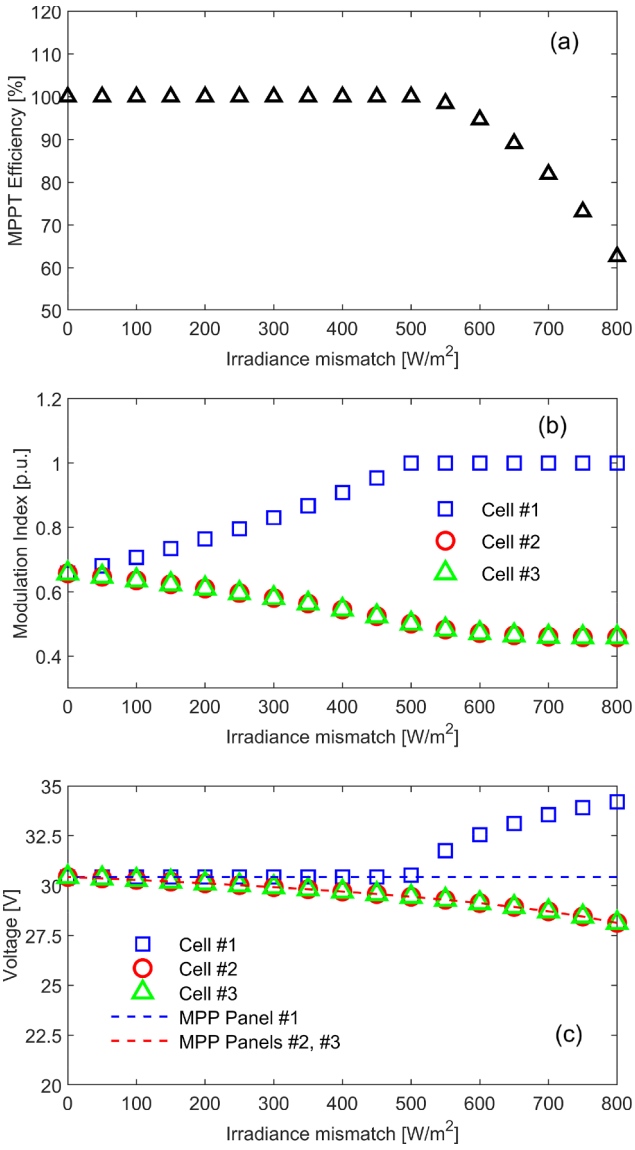

Fig. 9. Effect of mismatch: (a) global MPPT efficiency, (b) modulation indexes, (c) operating and MPP voltages for the three cells w.r.t. the irradiance mismatch.

threshold. The control action affects the MPPT efficiency, which falls to 60% at an irradiance mismatch of 800 W/m^2 (see Fig. 9.a). The whole system properly operates and all the cells modulate in linear region, thus no significant harmonic distortion on the grid current is expected.

Nevertheless, the constraint on the modulation index can be relaxed. The following analysis investigates the possibility to improve the MPPT efficiency by imposing for the modulation index an upper limit greater than 1.

Indeed, the whole system properly operates even if the modulation index of the power cells overcomes the limit of linear region, that is when the overmodulation occurs.

To better illustrate the improvements due to an enlargement of the allowed range for m_i, the previous analysis is repeated by varying the upper limit between 0.9 and 1.2. The results are shown in Fig. 10.

It can be deduced that, for increasing values of the upper limit, power cells track the MPP even in case of a larger mismatch (see Fig. 10.c), thus improving MPPT efficiency (see Fig. 10.a). Moreover, even if the modulation index saturates to its upper limit (e.g., panel #1 in Fig. 10.b), the corresponding operating voltage decreases by increasing m_i; therefore, the power cell operates closer to the MPP, so

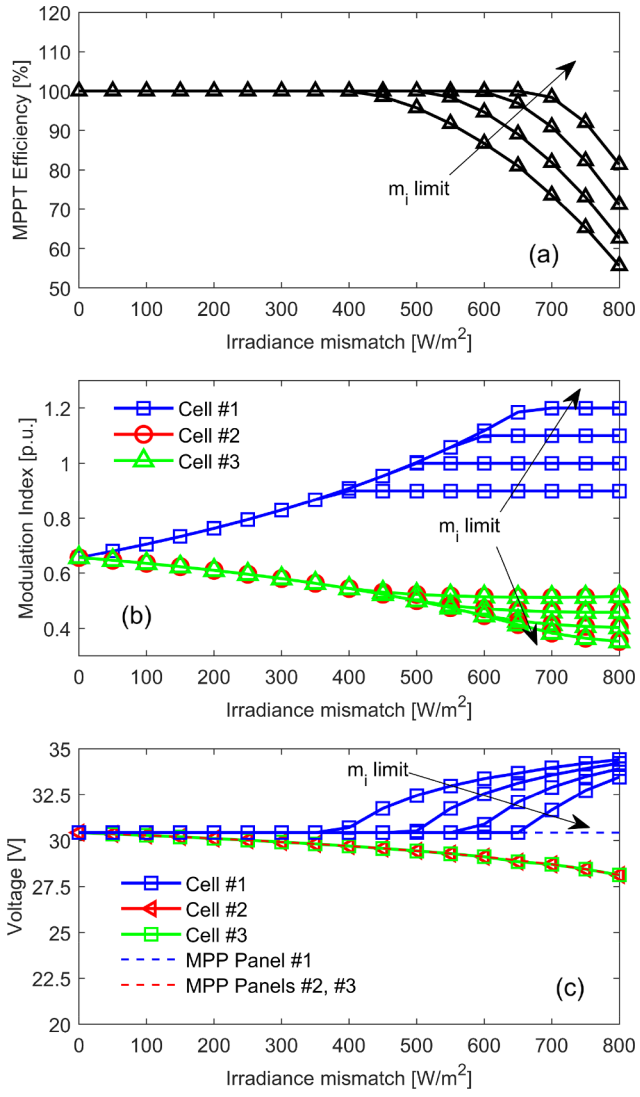

Fig. 10. Extension of m_i upper limit: (a) global MPPT efficiency, (b) modulation indexes for the three cells w.r.t. the irradiance mismatch and for the m_i upper limit value [0.9, 1, 1.1, 1.2], and (c) operating and MPP voltages.

improving the overall power extraction.

This approach cannot be used in case of conventional modulation methods (e.g., Multicarrier PWM), also in their modified versions, because of the detrimental effect on the harmonic content of the current injected to the grid [20,21]. On the contrary, as discussed in Section 3.3, with the proposed hybrid modulation, the most powerful cell is able to operate in the overmodulation region without significant effects on the current distortion, although it cannot reach the square wave operation due to the used switching scheme (including the zero switching state), which poses an upper limit to the maximum allowed modulation index. In the following section, the choice of the proper upper limit of m_i for the implemented prototype is discussed.

5. Experimental results

A laboratory prototype (see Fig. 11) of a sevenlevel PVmodule CHB inverter was built to prove the validity of the proposed design and control approach. Each power cell was equipped with four power MOSFET (IRFB4127PbF) with a breakdown voltage of 200 V and a continuous drain current of 54 *A* at $T_j = 100$ °C. The capacitance of the dclink capacitor was 4.6 *mF*. Each cell was fed by a PV simulator Ametek Elgar TerraSAS with a maximum rated power of 800 W (i.e.

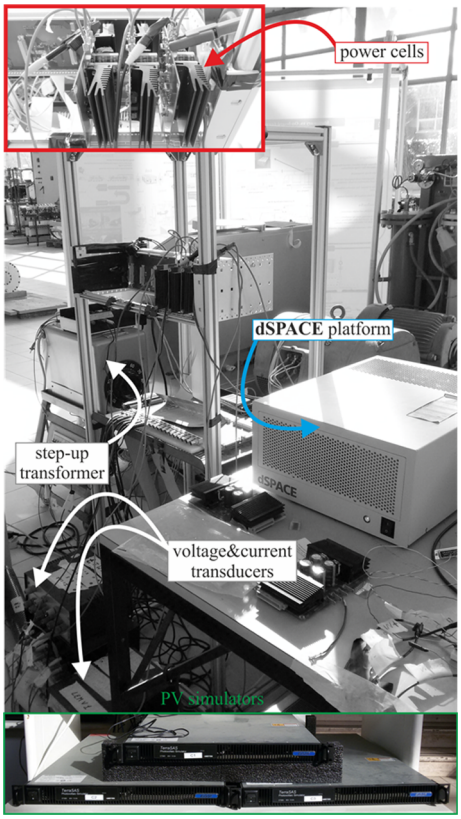

Fig. 11. Laboratory prototype.

80 V, 10 *A*). Each PV simulator was programmed to supply the IV profile of an individual PV module, with $P_{MPP} = 150$ W corresponding to $V_{MPP} = 29.5$ V and $I_{MPP} = 5$ *A* at STC. According to the IV curves in the irradiation range of [200 W/m^2, 1000 W/m^2], the lower boundary, v_{pv_min}, of the MPPT range was set to 24.5 V.

A stepup transformer was needed to interface the inverter output with the grid to meet the grid peak voltage. The transformer exhibited a secondary side voltage amplitude of about 43 V_{rms} in agreement with the MPPT range and the nominal input power of 450 W at an overall voltage of 88.5 V. Moreover, the line filter inductance *L* of 5 *mH* was used. The used switching frequency for the PWM is 5 kHz.

A realtime hardware platform dSpace ds1006 equipped with ds5203 (with onboard Field Programmable Gate Array (FPGA) Xilinx Virtex5) and an additional piggyback module providing 32 digital I/O, 12 A/D and 12 D/A channels was exploited to implement the control law. The design of the control circuit was realized in the Matlab/Simulink environment integrated with XSG (Xilinx System Generator) tool and dSpace RTI (RealTime Interface). The most part of the control was directly implemented on the FPGA by means of both IP blocks and custom Verilog modules. The main FPGA clock frequency is $f_{clk} = 100$ MHz. The module implementing the MPPT algorithm is executed at every $T_{MPPT} = 50$ ms. The MPPT period mainly depends on the rated power of the PV generator and on the input capacitor size. In particular, it should be ensured that the PV voltage reaches its reference voltage within the MPPT period. It is worth noting that the adopted MPPT time period (i.e., $T_{MPPT} = 50$ ms) is the lower one which allows to be in compliance with the aforementioned constraint.

On the other hand, the module implementing the sorting algorithm represents the bottleneck of our control in terms of timing. It should be guarantee that the sorted vector is obtained within the time interval T_{sort}, at the end of which the operating modes of the power cells are updated. Moreover, the T_{sort} cannot be increased too much to avoid a deterioration of the tracking behavior, while it must be set to a neighbor integral multiple of the switching period. For this purpose, the

computational time needed to obtain the sorted vector must be much lower than T_{sort}. In our case ($N = 3$), this time period is equal to $3T_{clk}$, so no limiting the choice of the T_{sort}. Nevertheless, its maximum computational time complexity can be $O(N^2)$, being N the number of elements to sort.

Therefore, by considering a realistic number N of cells (e.g., in single-phase application it will be less than 20), the high operating frequency of the FPGA allows to perform the sorting with no impact on the system dynamics.

To verify the system performance three different scenarios were considered: static uniform and mismatch in both static and dynamic conditions.

5.1. Uniform Conditions

In the first experiment, to emulate PV sources under uniform irradiance conditions, the three PV simulators were set at the same irradiance level, and the steady state behavior of the system was considered. The tests were repeated for different irradiance values, starting from 1000 W/m^2 down to 100 W/m^2.

Measured MPPT, conversion, and global efficiencies, along with THD, are reported in Fig. 12. As can be seen in Fig. 12.a) the MPPT efficiency was always greater than 98%; the degradation at high irradiance levels was likely due to the 100 Hz oscillation, whose amplitude increases with the input power. It is worth noting that the conversion efficiency linearly decreases as the power increases. This behavior was related to the increased power losses on the semiconductor devices, mainly dominated by the static losses of freewheeling diodes. Fig. 12.b) shows the good system performance in terms of THD, whose values accomplished grid requirements in all the considered cases.

For the case corresponding to the highest irradiance value (i.e., 1000 W/m^2), the MPP tracking behavior for the three PV sources, reported in Fig. 13.a, shows that, as expected in uniform condition, each cell operates close to the MPP voltage of 29.5 V. The modulation indexes achieve the expected value of 0.7 (i.e., (V_{grid} /3) / V_{MPP})) for all the power cells, as shown in Fig. 13.b). At ac side, the grid current results sinusoidal in phase with the grid voltage (see Fig. 14), thus leading to a satisfying power factor and a low value of THD (i.e., about 1%).

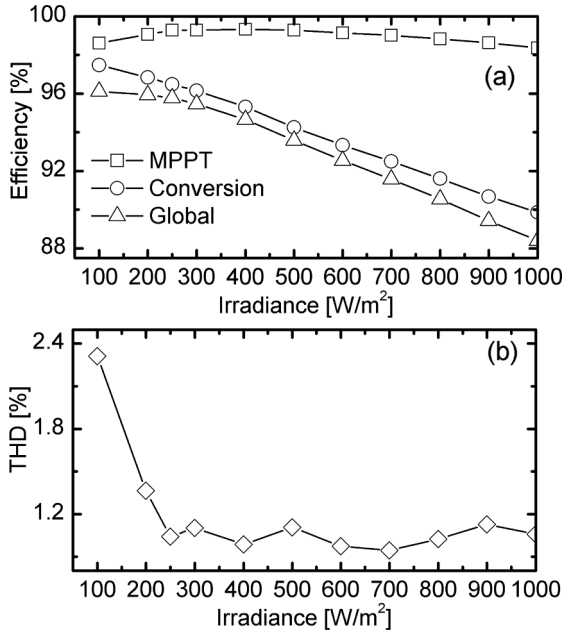

Fig. 12. Uniform conditions: (a) global, conversion and MPPT efficiency of the laboratory prototype as function of the irradiance of the PVGs; (b) THD behavior is also shown.

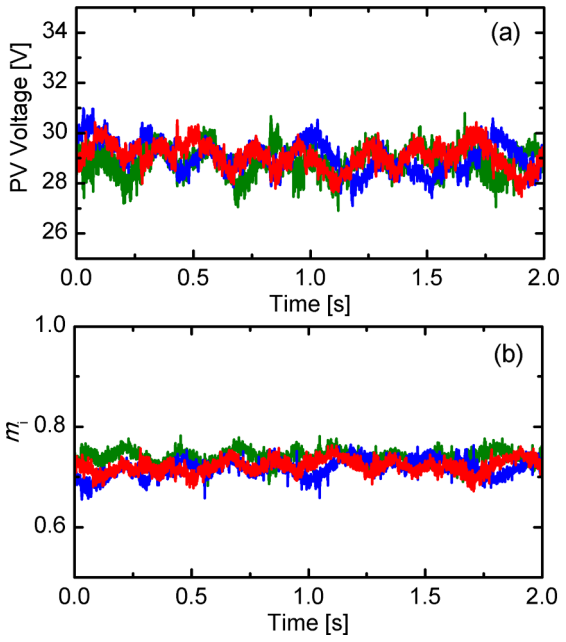

Fig. 13. PVGs irradiance of 1000 W/m^2: steady state behavior of (a) input operating voltages and (b) corresponding modulation indexes of the three power cells (blue, cell #1; red, cell #2; green, cell #3) in an observation window of 2 s. (For interpretation of the references to colour in this figure legend, the reader is referred to the web version of this article.)

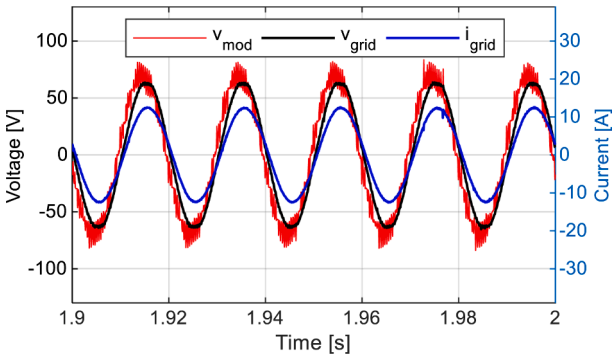

Fig. 14. PVGs irradiance of 1000 W/m^2: steady state behavior of grid current (blue line), modulated voltage (red line), and the grid voltage in an observation window of [1.9 s, 2 s]. (For interpretation of the references to colour in this figure legend, the reader is referred to the web version of this article.)

5.2. Mismatch Conditions

The second experiment provided information about the system behavior under deep mismatch conditions. The effect of mismatch among PV sources on the MPP tracking was investigated for different values of the modulation index upper limit.

According to the theoretical analysis discussed in Section 4, tests were performed under the worst irradiance conditions, obtained by supplying two cells with 250 W/m^2, and the third with 1000 W/m^2. The value of 250 W/m^2 corresponds to a solar panel only subject to the diffuse component of the sunlight; such a condition occurs when, in a *clearsky* sunny day, the solar panel is completely shielded from direct light.

Fig. 15.a) shows the behavior of the modulation indexes m_i for the different value of the upper limit (represented by the black dashed line in the figure). As expected, the modulation index of the cell #1 (i.e., the

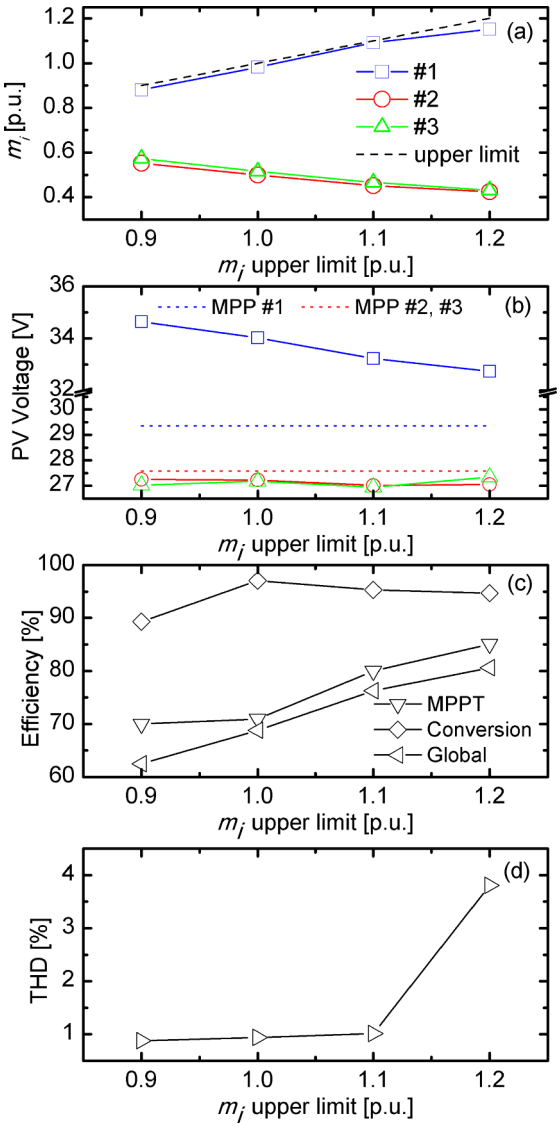

Fig. 15. Experimental extension of m_i upper limit in case of mismatch: (a) modulation indexes; (b) operating and MPP voltages for the three cells; (c) global, conversion and MPPT efficiencies, and (d) THD for the m_i upper limit value [0.9, 1, 1.1, 1.2].

cell with higher input power/irradiance) grew with respect to the other cells (cells with weaker power/ irradiance) up to reach the upper limit when this latter assumed the values of 0.9, 1, and 1.1.

In such cases, the modulation index m_1 exceeds the upper limit, due to the P&O algorithm, so activating the control section which increases the PV reference voltage of a quantity equal to $\Delta_{pv} = 0.5$ V until the modulation index falls again below the limit. The recurrence of such behavior establishes a limit cycle around the modulation index threshold (i.e., the fixed upper limit) as shown in Figs. 16 and 17, for the threshold values of 1 and 1.1, respectively. Cell #1 operates correctly at a higher voltage w.r.t. V_{MPP} (as also shown in Fig. 15.b) in both the cases.

Nevertheless, by relaxing the threshold from 1 to 1.1, the control allows cell#1 to achieve a lower operating voltage closer to the MPP, thus resulting in a 10% increase of the overall MPPT efficiency (see Fig. 15.c)).

As can be inferred from Fig. 15.d), the proposed modulation technique allows to operate the system in the overmodulation region with no relevant effect on the THD, which always remains in the required limits for gridconnected application.

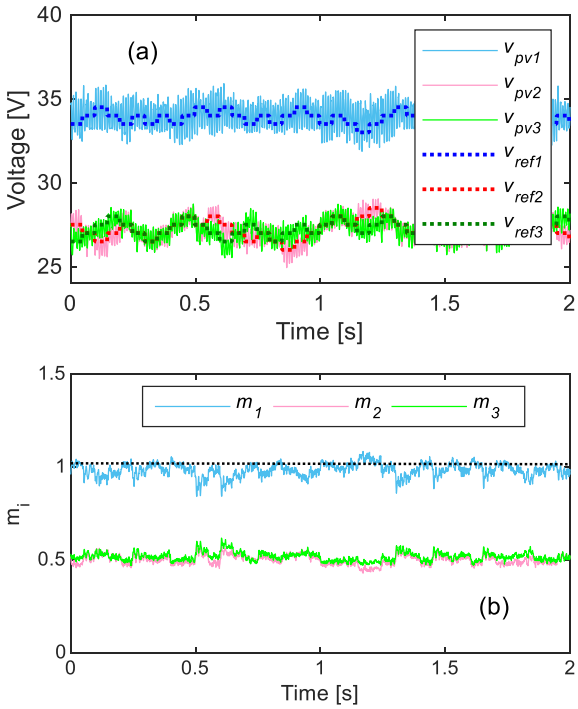

Fig. 16. m_i limit 1: steady state behavior of (a) input operating voltages and reference voltages, and (b) corresponding modulation indexes of the three power cells (blue, cell #1; red, cell #2; green, cell #3) in an observation window of 2 s. (For interpretation of the references to colour in this figure legend, the reader is referred to the web version of this article.)

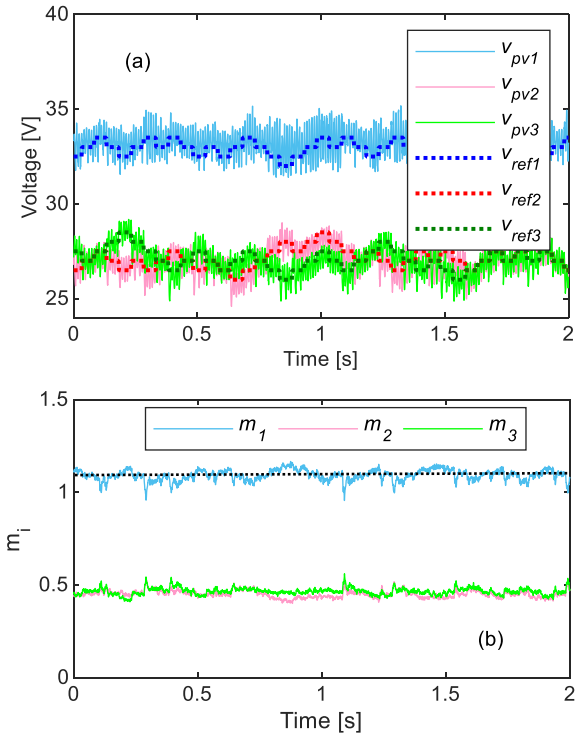

Fig. 17. m_i limit 1.1: steady state behavior of (a) input operating and reference voltages, and (b) corresponding modulation indexes of the three power cells (blue, cell #1; red, cell #2; green, cell #3) in an observation window of 2 s. (For interpretation of the references to colour in this figure legend, the reader is referred to the web version of this article.)

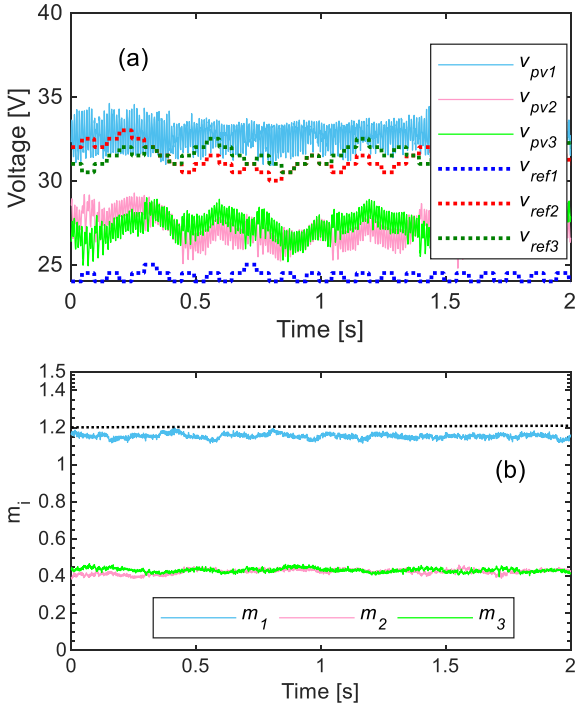

Fig. 18. m_i limit 1.2: steady state behavior of (a) input operating voltages and reference voltages, and (b) corresponding modulation indexes of the three power cells (blue, cell #1; red, cell #2; green, cell #3) in an observation window of 2 s. (For interpretation of the references to colour in this figure legend, the reader is referred to the web version of this article.)

By analyzing the trends in Fig. 15, it could be erroneously argued that an improvement in terms of MPPT efficiency can be obtained by relaxing the upper limit of the modulation index up to the theoretical maximum value of $4/\pi$, but the effective maximum achievable value depends on the used modulation technique.

It is worth noting that the proposed hybrid modulation strategy, as already discussed in Section 3.3, implies that at least one cell per cycle is in PWM mode, while the others can assume the remaining modes (i.e., 0 mode, cell bypassed; ± 1 mode, cell inserted). As a consequence, the cells cannot reach the squarewave operation ($m_i = 4/\pi$), thus limiting the maximum modulation index to a value depending on the specific operating configuration: grid peak voltage, instantaneous input power, line inductance value and IV characteristics of used PV sources. In particular, in the considered configurations, the system operating range can be extended to a maximum value of the modulation index lower than 1.2.

In fact, as shown in Fig. 18, by imposing an upper limit of 1.2, the more powerful cell reaches its maximum power capability with a modulation index lower than 1.2 (see Fig. 18.b), while reaching its minimum allowed operating voltage (see Fig. 18.a). As a consequence, the modulation index control never acts (i.e., the upper limit is never exceeded), so the voltage reference is still provided by P&O algorithm, which erroneously asks for further decreases of the voltage to track the MPP. In such a case, the voltage reference achieves the minimum allowed value of $v_{pv,\min}$, always located at lower voltage w.r.t. the MPP. The main control loop keeps to zero the input PI error by compensating the negative voltage error of cell #1 with the positive ones of the other cells. This means that the system continues to operate but the cells are not able to track their references.

In fact, the system is able to inject a sinusoidal current to the grid, but it is no more under control and the THD value increases noticeably w.r.t. the stable operating conditions considered during other experiments (see Fig. 15.d).

According to the above discussion, a suitable choice of the upper limit is in the range [1.1 ÷ 1.2] with the aim of guaranteeing an extended operating range of the CHB inverter due to a proper operation of the system control.

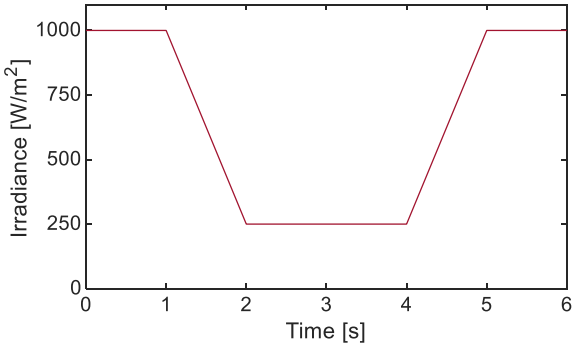

Fig. 19. Irradiance profile of PV simulator (cell #3).

5.3. Dynamic Mismatch Conditions

The third experiment was performed to investigate the behavior of the system under dynamic mismatch conditions.

The idea is to dynamically force the system to move from a uniform condition to a heavy mismatch condition (the worst case considered in the previous experiment). The irradiance of the PV simulators supplying cells #1 and #2 is set to the constant value of 250 W/m^2 during the whole test period. On the contrary, the PV simulator supplying cell #3 tracks the dynamic irradiance profile depicted in Fig. 19 (i.e., the irradiance cycle). As it is shown, the irradiance value switches between 1000 W/m^2 and 250 W/m^2 with dwell time of 2 s and rise/fall time of 1 s.

The effect of dynamic mismatch among PV sources on the MPP tracking accuracy and on the quality of the output power was investigated for three different values of the modulation index upper limit, namely 1.0, 1.1 and 1.2. The dynamic MPPT efficiency is averaged over the 15 irradiance cycles, while the PF and the THD are evaluated over a time window corresponding to a single irradiance cycle.

In Figs. 21(a) and 20(a) the behavior of the input operating voltage of the three cells are shown compared to the respective reference voltages. As expected, the reference voltages of cells #1 and #2 are not perturbated by the irradiance variation involving cell #3, and the corresponding input voltages properly track the references. On the contrary, for cell #3, the MPPT algorithm, based on P&O, is affected by a degradation of performance close to the rising/falling irradiation edges. Moreover, due to the modulation index control, the input voltage experiences a sudden increase, thus moving the operating point far from the MPP. Nevertheless, by comparing Figs. 21(a) and 20(a), the increase of the operating voltage results mitigated by extended the upper limit from 1 to 1.1.

It is important to note that at ac side, the current control loop well performs even during the irradiance transitions and the grid current results sinusoidal in phase with the grid voltage (see Figs. 21(a) and 20(a)), thus leading to a satisfying power factor and a low value of THD.

In Fig. 22(a) the behavior of the input operating voltage of the three cells are shown compared to the respective reference voltages for the upper limit set to 1.2. It is easily inferred that the inverter does not control anymore the input voltage of the cells, which do not track the corresponding reference voltages.

Table 1 resumes the experimental results obtained during dynamic tests. It can be inferred that, for the upper limit of the modulation index set to 1 and 1.1, cell #1 and #2 stably operate near their own MPP, while cell #3 is forced to operate far from the MPP due to modulation index control, thus affecting the global MPPT efficiency. It is worth

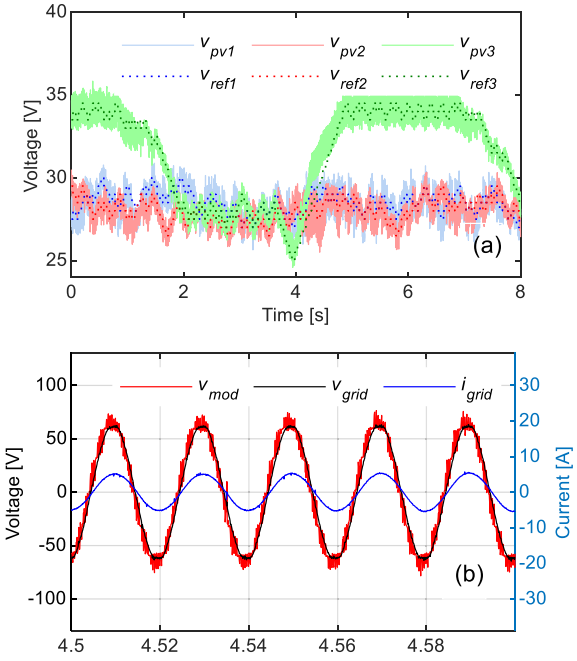

Fig. 20. m_i limit 1: (a) input operating and reference voltages in an observation window of 8 s (b) grid voltage, grid current, and inverter modulating voltages in an observation window of 0.1 s during the rising edge of the irradiance profile in Fig. 19.

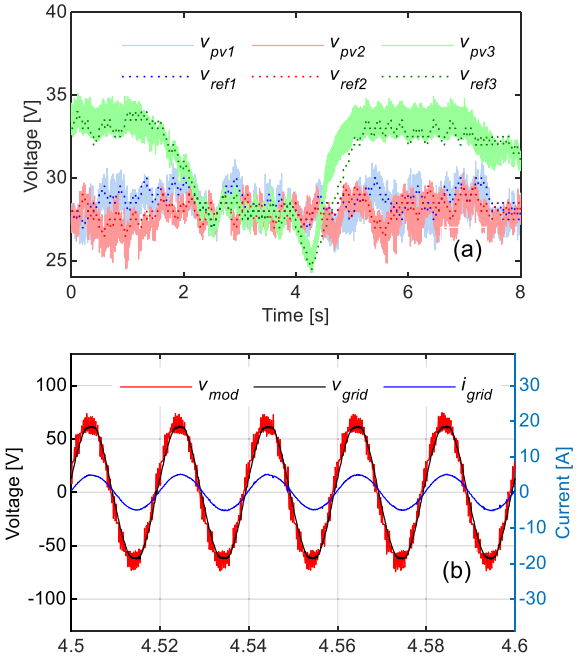

Fig. 21. m_i limit 1.1: (a) input operating and reference voltages in an observation window of 8 s (b) grid voltage, grid current, and inverter modulating voltages in an observation window of 0.1 s during the rising edge of the irradiance profile in Fig. 19.

noting that the MPPT efficiency of cell #3 improves, as expected, by relaxing the upper limit by passing from 1 to 1.1.

For the upper limit of the modulation index set to 1.2, the MPPT efficiency experiences a further increase, reaching the 82.7%, thus enhancing the global MPP up to the 98.3%. On the other hand, the converter experience a lack of control due to the mechanism discussed in Section 5.2, leading to the failure of the MPPT, while the THD reaches the significant value of 1.3.

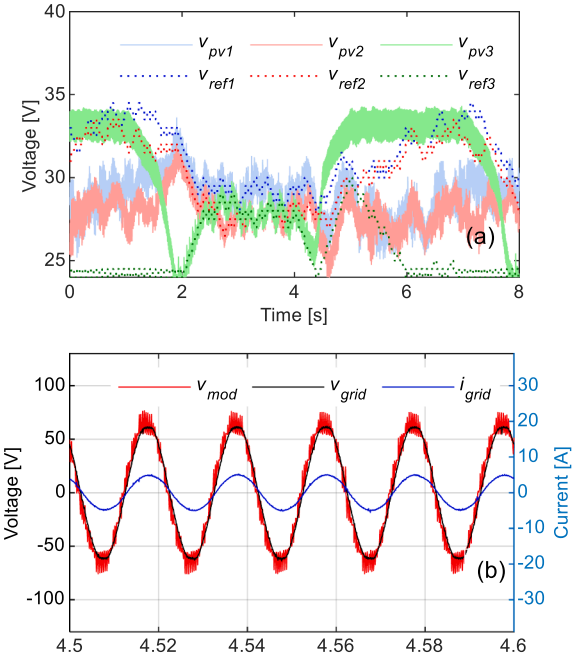

Fig. 22. m_i limit 1.2: (a) input operating and reference voltages in an observation window of 8 s (b) grid voltage, grid current, and inverter modulating voltages in an observation window of 0.1 s during the rising edge of the irradiance profile in Fig. 19.

Table 1
Experimental results under dynamic mismatch condition: MPPT efficiency, Power Factor (PF), THD.

m_i upper limit	MPPT efficiency [%]				Power Factor	THD [%]
	Cell #1	Cell #2	Cell #3	Global		
1	99.3	99.3	66.8	77.8	0.98	0.3
1.1	99.3	99.2	77.7	83.0	0.97	0.3
1.2	98.2	98.6	82.7	98.3	0.97	1.3

6. Conclusions

This paper has been focused on the control and modulation of a PV module-level CHB inverter. The advantages and drawbacks of the used circuit topology have been highlighted. In particular, the tradeoff between the extended circuit operating range and the harvesting of the maximum available PV power has been considered also in case of heavy mismatch conditions (i.e., worst case).

A numerical analysis has been conducted to show the operating limits of the proposed architecture and how these limits can be theoretically overcome by increasing the modulation index, while assuring proper operation with no degradation of MPPT efficiency, at least until heavy mismatch occurs. Obtained results prove that the enlargement of the modulation index boundary allows the cells to properly handle the corresponding PV power in an extended range of mismatch configurations.

An enhanced distributed maximum power point tracking (DMPPT) algorithm along with an improved hybrid modulation method has been implemented to extend the operating range of the seven-level PV CHB inverter. Experimental results clearly show that the system is fully functional in different operating conditions included the case of deep mismatch. In this latter case, the increase of the modulation index upper limit determines improved system performance in terms of efficiency and power quality, thus proving the effectiveness of the proposed control and modulation method.

It has been also highlighted a limitation of the proposed hybrid

modulation, which is not able to drive the cells in squarewave operation, thus requiring the choice of the suitable upper limit of the modulation index.

Declaration of Competing Interest

The authors declare that they have no known competing financial interests or personal relationships that could have appeared to influence the work reported in this paper.

Appendix A. Supplementary material

Supplementary data to this article can be found online at https://doi.org/10.1016/j.ijepes.2020.105892.

References

[1] Hammons TJ. Integrating renewable energy sources into European grids. Int J Electr Power Energy Syst 2008;30(8):462–75.
[2] Kumar Nayan, Saha Tapas Kumar, Dey Jayati. Modeling, control and analysis of cascaded inverter based grid-connected photovoltaic system. Int J Electr Power Energy Syst 2016;78:165–73.
[3] Blaabjerg Frede, Ionel Dan M. Renewable energy devices and systems – state-of-the-art technology, research and development, challenges and future trends. Electr Power Compon Syst 2015;43(12):1319–28.
[4] Sera D, Mathe L, Kerekes T, Spataru SV, Teodorescu R. On the perturb-and-observe and incremental conductance MPPT methods for PV systems. IEEE J Photovoltaics 2013;3(3):1070–8.
[5] Kouro S, Leon JI, Vinnikov D, Franquelo LG. Grid-connected photovoltaic systems: an overview of recent research and emerging PV converter technology. IEEE Ind Electron Mag 2015;9(1):47–61.
[6] Femia N, Lisi G, Petrone G, Spagnuolo G, Vitelli M. Distributed maximum power point tracking of photovoltaic arrays: Novel approach and system analysis. IEEE Trans Ind Electron 2008;55(7):2610–21.
[7] Jafarian H, Bhowmik S, Parkhideh B. Hybrid current-/voltage-mode control scheme for distributed AC-stacked PV inverter with low-bandwidth communication requirements. IEEE Trans Ind Electron 2018;65(1):321–30.
[8] Vidales B, Monroy-Morales José Luis, Rodrìguez-Rodriguez JR, Madrigal M, Torres-Lucio D. A transformerless topology for a micro inverter with elevation factor of 1: 10 for photovoltaic applications. Int J Electr Power Energy Syst 2019;109:504–12.
[9] Goetz Stefan M, Wang Chuang, Li Zhongxi, Murphy David LK, Peterchev Angel V. Concept of a distributed photovoltaic multilevel inverter with cascaded double H-bridge topology. Int J Electr Power Energy Syst 2019;110:667–78.
[10] Balato Marco, Vitelli Massimo. Optimization of distributed maximum power point tracking PV applications: The scan of the Power vs. Voltage input characteristic of the inverter. Int J Electr Power Energy Syst 2014;60:334–46.
[11] Spagnuolo G, et al. Renewable energy operation and conversion schemes: a summary of discussions during the seminar on renewable energy systems. IEEE Ind Electron Mag 2010;4(1):38–51.
[12] Tran Quang-Tho, Truong Anh Viet, Le Phuong Minh. Reduction of harmonics in grid-connected inverters using variable switching frequency. Int J Electr Power Energy Syst 2016;82:242–51.
[13] Villanueva, Correa P, Rodriguez J, Pacas M. Control of a single-phase cascaded H-bridge multilevel inverter for grid-connected photovoltaic systems. IEEE Trans Ind Electron 2009;56(11):4399–406.
[14] Chavarria J, Biel D, Guinjoan F, Meza C, Negroni JJ. Energy-balance control of PV cascaded multilevel grid-connected inverters under level-shifted and phase-shifted PWMs. IEEE Trans Ind Electron 2013;60(1):98–111.
[15] Kouro S, Wu B, Moya A, Villanueva E, Correa P, Rodriguez J. Control of a cascaded H-bridge multilevel converter for grid connection of photovoltaic systems. IECON. 2009. p. 3976–82.
[16] Eskandari A, Javadian V, Iman-Eini H, Yadollahi M. Stable operation of grid connected Cascaded H-Bridge inverter under unbalanced insolation conditions. Proc. 3rd International Conference EPECS. 2013. p. 1–6.
[17] Rezaei MA, Farhangi S, Iman-Eini H. Enhancing the reliability of single-phase CHB-based grid-connected photovoltaic energy systems. PEDSTC. 2011. p. 117–22.
[18] Marquez A, et al. Variable-angle phase-shifted PWM for multilevel three-cell cascaded H-bridge converters. IEEE Trans Ind Electron 2017;64(5):3619–28.
[19] Xiao B, Hang L, Mei J, Riley C, Tolbert LM, Ozpineci B. Modular Cascaded H-Bridge Multilevel PV Inverter With Distributed MPPT for Grid-Connected Applications. IEEE Trans Ind Appl 2015;51(2):1722–31.
[20] Miranbeigi M, Iman-Eini H. Hybrid Modulation Technique for Grid-Connected Cascaded Photovoltaic Systems. IEEE Trans Ind Electron 2016;63(12):7843–53.
[21] Iman-Eini Hossein, Tennakoon Sarath B. Investigation of a cascaded H-bridge photovoltaic inverter under non-uniform insolation conditions by hardware in-the-loop test. Int J Electr Power Energy Syst 2019;105:330–40.
[22] Xiao B, Filho F, Tolbert LM. Single-phase cascaded H-bridge multilevel inverter with nonactive power compensation for grid-connected photovoltaic generators. Proc. ECCE. 2011. p. 2733–7.
[23] Filho F, Tolbert LM, Cao Yue, Ozpineci B. Real-time selective harmonic minimization for multilevel inverters connected to solar panels using artificial neural network angle generation. IEEE Trans Ind Appl 2011;47(5):2117–24.
[24] Prabaharan N, Palanisamy K. Analysis and integration of multilevel inverter configuration with boost converters in a photovoltaic system. Energy Convers Manage 2016;128:327–42.
[25] Coppola M, Di Napoli F, Guerriero P, Iannuzzi D, Daliento S, Del Pizzo A. An FPGA-based advanced control strategy of a GridTied PV CHB inverter. IEEE Trans Power Electron 2016;31(1):806–16.
[26] Franquelo LG, Rodriguez J, Leon JI, Kouro S, Portillo R, Prats MAM. The age of multilevel converters arrives. Indus Electron Mag, IEEE 2008;2(2):28–39.
[27] Rodriguez J, Bernet S, Bin Wu, Pontt JO, Kouro S. Multilevel voltage-source-converter topologies for industrial medium-voltage drives. IEEE Trans Indus Electron 2007;54(6):2930–45.
[28] Guerriero P, Coppola M, Di Napoli F, Brando G, Dannier A, Iannuzzi D, et al. Three-phase PV CHB inverter for a distributed power generation system. Appl Sci 2016;6(10):287.
[29] Celentano L. Tracking controllers design of references with bounded derivative. Appl Math Sci 2012;6(95):4709–28.